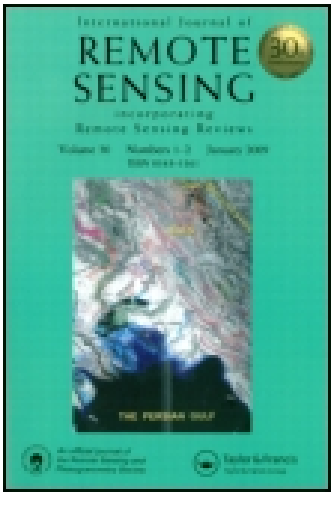

International Journal of Remote Sensing

Publication details, including instructions for authors and subscription information:
http://www.tandfonline.com/loi/tres20

A study of NOAA particle flux sensitivity to solar activity and strategies to search for correlations among satellite data and earthquake phenomena

Cristiano Fidani [a], Roberto Battiston [a b], William J. Burger [a] & Livio Conti [c]

[a] National Institute of Nuclear Physics, Perugia, Italy

[b] Department of Physics, Perugia University, Perugia, Italy

[c] Department of Physics 'E. Amaldi', Roma Tre University, Roma, Italy

Published online: 13 Feb 2012.

To cite this article: Cristiano Fidani, Roberto Battiston, William J. Burger & Livio Conti (2012) A study of NOAA particle flux sensitivity to solar activity and strategies to search for correlations among satellite data and earthquake phenomena, International Journal of Remote Sensing, 33:15, 4796-4814, DOI: 10.1080/01431161.2011.638337

To link to this article: http://dx.doi.org/10.1080/01431161.2011.638337

International Journal of Remote Sensing
Vol. 33, No. 15, 10 August 2012, 4796–4814

Taylor & Francis
Taylor & Francis Group

A study of NOAA particle flux sensitivity to solar activity and strategies to search for correlations among satellite data and earthquake phenomena

CRISTIANO FIDANI*†, ROBERTO BATTISTON†‡, WILLIAM J. BURGER† and LIVIO CONTI§

†National Institute of Nuclear Physics, Perugia, Italy
‡Department of Physics, Perugia University, Perugia, Italy
§Department of Physics 'E. Amaldi', Roma Tre University, Roma, Italy

The data provided by particle and plasma physics satellites represent a potentially important source of information for the study of seismic activity on a planetary scale. The increasing number of observations concerning meteorological and telecommunication satellites indicate that particle precipitation, infrared emission and anomalies in communication links may be associated, although not yet in a systematic manner, with earthquakes. Several studies have attempted to correlate satellite observations with seismic phenomena, however, few present statistically significant results. In this study, the National Oceanic and Atmospheric Administration (NOAA) electron flux measurements are used. With respect to previous efforts, we define contiguous particle bursts (PBs) and study their autocorrelations; the latter may be used to distinguish the origin of the observed fluctuations. The goal is to combine data from satellite and Earth surface measurements to better understand the potential of remote sensing of seismic phenomena. In this context, we stress the importance of international coordination, shared databases and the harmonization of existing methodologies.

1. Introduction

The study of earthquake-related ionospheric phenomena was stimulated by the ionospheric disturbances observed around the time of the great Alaskan earthquake (Davies and Baker 1965) on 28 March 1964. Subsequent satellite measurements (Larkina *et al.* 1983) have confirmed the relevance of this approach, which provides medium and far field views of lithosphere phenomena with respect to the earthquake site. Estimations of the size of the earthquake preparation zone range from 150 km for magnitude 5 earthquakes to more than 2500 km for magnitude 8 (Dobrovolsky *et al.* 1979), which are the distances from the epicentre. A terrestrial observation of non-seismic phenomena linked to strong earthquakes produce local perturbations, which are strongly affected by several land and atmospheric variables, including anthropogenic disturbances. A low earth orbit (LEO) satellite, at an altitude of 200–2000 km, provides, in principle, a platform of observation extending over the entire affected region (Parrot 1995).

*Corresponding author. Email: c.fidani@virgilio.it

International Journal of Remote Sensing
ISSN 0143-1161 print/ISSN 1366-5901 online © 2012 Taylor & Francis
http://www.tandf.co.uk/journals
http://dx.doi.org/10.1080/01431161.2011.638337

Rock micro-fracturing preceding a seismic rupture may cause local surface deformation fields, rock dislocations, charged particle generation and motion, electrical conductivity changes, gas emission, fluid diffusion and electrokinetic, piezomagnetic and piezoelectric effects (Varotsos 2001). Charge carriers could be activated in dry rocks mainly by increasing external stress (Freund 2000). These processes have been considered as the main sources of the so-called seismo-electromagnetic (SEM) emissions consisting of broadband (from microhertz to a few tens of megahertz) electromagnetic (EM) fields observed at the Earth's surface and in the near-Earth space, the neutral and ionized atmosphere, and the magnetosphere. LEO satellite observations provide information on ionospheric and magnetospheric perturbations possibly caused by pre-seismic EM waves and, in particular, radiation belt particle precipitations (Aleksandrin *et al.* 2003), infrared emissions (Yurur 2006), temperature and density variations of the ions and electrons of the ionospheric plasma (Sarkar *et al.* 2007), and electric and magnetic field fluctuations (Bhattacharya *et al.* 2009).

No clear causal relationship has been established experimentally between earthquake phenomena and the previously cited physical processes. An explanation for the observed perturbations in the near-Earth space in terms of the propagation of SEM waves through the atmosphere and magnetosphere and/or gas diffusion remains hypothetical. Recent results from the very low frequency (VLF) satellite study reveal a small decrease in wave intensity before strong earthquakes over their epicentres (Nemec *et al.* 2009), which imply the EM field perturbations are not the only phenomenon affecting the near-Earth space. The influence of atmospheric EM emissions of anthropogenic origin or during thunderstorm activity, atmospheric circulation, and the effects of the Sun and cosmic rays on the observed particle fluxes, must be filtered to obtain a definitive conclusion from the data.

In this work, we present a methodology to distinguish candidate flux variations from the backgound, i.e. variations of non-seismic origin. The method has been applied to the electron counting rates (CRs) of the Polar Orbital Environmental Satellites (POES) of the National Oceanic and Atmospheric Administration (NOAA). Section 2 contains a description of the particle detectors of the POES, which are compared to the particle detectors of other satellites whose data have been used to search for correlations with seismic activity. Section 3 discusses the physics of particle precipitation from the Earth's radiation belts. Particle precipitation results in an increase of the particle fluxes observed in LEO. Section 4 presents the analysis and results of the NOAA data. Section 5 provides the conclusions and general observations.

2. Satellite instruments

In the last decade, different satellite instruments for the study of earthquake effects have been proposed. To study systematically the EM waves of lithospheric origin and related ionospheric changes, the proposed devices include electric and magnetic probes, charged particle detectors and thermal plasma analysers. Refined meteorological and GPS satellite technology provide additional ready-to-use tools for seismic correlation research.

In this work, we focus on particle precipitation. The first satellite dedicated to this objective was the DEMETER (Detection of Electro-magnetic Emissions Transmitted from Earthquake Regions) satellite (Parrot 1995), which was launched in 2004 and is still operational. The data of other satellites have been used to search for correlations between particle flux variations and seismic activity. In particular, a correlation has

been reported between the high-energy electron flux changes observed with the Solar, Anomalous and Magnetospheric Particle Explorer (SAMPEX) (Sgrigna *et al.* 2005). The ARINA payload (Bakaldin *et al.* 2007), launched with the Pamela magnetic spectrometer (Casolino *et al.* 2008), is a device designed to study the correlation between particle precipitation and earthquakes. Pamela and the Alpha Magnetic Spectrometer (AMS) (Aguilar *et al.* 2002) are particle detectors that provide flux measurements of the trapped particles at higher energies. In principle, the data of these astrophysics detectors may also be exploited.

2.1 *DEMETER IDP*

The micro-satellite DEMETER has a heliosynchronous, low polar orbit at an altitude of 710 km, chosen to survey almost all the seismically active regions of the globe (Sauvaud *et al.* 2006). The particle detector (Instrument for the Detection of Particles – IDP) consists of a 2.5 cm-diameter, 1 mm-thick fully depleted silicon diode that provides a total energy measurement for electrons between 70 and 1000 keV. An aluminum collimator defines the opening angle of 32°; the geometric factor is 1.2 cm^2 sr. Since the detector is pointed perpendicularly to the orbital plane, the pitch angle of the detected particles is close to 90°.

The signal output of the silicon is sent to both a low-noise charge-sensitive preamplifier and a shaping amplifier, to operate at rates of ∼0.5 MHz. The signals are digitized by an 8-bit ADC (energy range from 70 keV to 2.34 MeV) with an energy resolution better than 8% for the electrons, which are stopped. In practice, the detector has two operational modes: a burst mode that provides an electron energy spectrum every second over the full 256 channel range (resolution better than 10 keV) and a routine mode that provides an energy spectrum of 128 channels over the full dynamic range every 4 seconds. Energy losses larger than 2.34 MeV are recorded in the last channel.

The importance of good energy resolution has been illustrated by the observation of structure, in the electron energy spectra recorded west of the South Atlantic Anomaly (SAA), consisting of a succession of 12 peaks between 150 keV and 1 MeV (Sauvaud *et al.* 2006).

2.2 *SAMPEX PET*

The Proton/Electron Telescope (PET) (Cook *et al.* 1993) of SAMPEX (Baker *et al.* 1993) consists of a stack of 12 circular Li-drifted silicon detectors with thicknesses ranging from 2 to 15 mm and diameters of 3.2–3.4 cm. A passive collimator and the first two detectors in the stack define the opening angle of the telescope (58°).

The signals of the silicon detectors are DC-coupled to charge-sensitive preamplifiers, shaping amplifiers and are digitized by 10-bit ADCs. The signals of five 5 mm-thick silicon sensors are summed together prior to digitization; a total of eight 10-bit words are present in the output of each event. The recorded signal levels, the specific and total energy losses, are compared with the known range–energy relations to identify protons, electrons and heavier nuclei.

The different detector combinations provide low- (1–4 MeV) and high- (4–20 MeV) energy electron channels with a geometric acceptance of ∼1.7 cm^2 sr. The CRs of the identified electrons, accumulated in 6-second intervals, are transmitted to the ground via telemetry. Similar rates are provided for protons in the energy ranges of 19–28 and 28–64 MeV.

The elliptical orbit of SAMPEX (Baker *et al.* 1993) has an inclination angle of 82° with altitudes between 520 and 670 km. The satellite payload also includes a magnetometer and particle detectors optimized for the detection of heavy ions and isotopes.

2.3 *NOAA MEPED*

The POES of the NOAA contain particle detectors that monitor fluxes of energetic ions and electrons entering the atmosphere, as well as the particle radiation environment at the altitude of the satellite (Davies 2007). The satellites are placed in polar orbit (inclination angles of ∼99°) at altitudes between 807 and 854 km (NOAA satellites 15–19).

The particle detectors (SEM-2) consist of the Total Energy Detector (TED) and the Medium Energy Proton and Electron Detector (MEPED) (Evans and Greer 2004).

The MEPED is composed of eight solid-state detectors that measure proton and electron fluxes from 30 keV to 200 MeV (including the radiation belt populations), energetic solar particle events (protons) and the low-energy portion of the galactic cosmic-ray population. The eight detectors consist of two proton telescopes that monitor the flux in five energy bands in the range 30 keV to 6.9 MeV, two electron telescopes that monitor the flux in three energy bands in the range 30 keV to 2.5 MeV, and four 'omni-directional' detectors sensitive to proton energies above 16 MeV.

Each electron telescope consists of a single 0.7 mm thick silicon surface barrier detector with a sensitive area of 25 mm^2. The silicon detectors are surrounded by aluminium and tungsten shielding to eliminate electrons (protons) with energies below 6(90) MeV. The opening angle aperture for the two telescopes is 30°. The geometric acceptances are 0.1 cm^2 sr. One telescope views at an angle of 9° with respect to the local zenith. The second telescope views in the orthogonal direction.

A discriminator amplitude level is set to an equivalent particle energy loss of 2.5 MeV. Signal levels below the 2.5 MeV threshold are pulse height analysed and sorted in three energy bands between 30 keV and 2.5 MeV. The electron rates in each energy band are determined every second. The electron detector telescopes are sensitive to proton energies between 210 keV and 2.7 MeV, consequently the computed electron fluxes should be corrected with the fluxes of the proton telescopes.

The relevant parameters of the SAMPEX, DEMETER and NOAA (MEPED) particle detectors are summarized in table 1. At present, the most significant correlation between flux variations and seismic activity has been reported in the upper electron energy range of the SAMPEX PET (Sgrigna *et al.* 2005).

Table 1. The principal characteristics of the particle detectors of the three satellites.

Class detector	Geometric factor (cm^2 sr)	Aperture (°)	Orbit		Pitch (°)	Electron energy range (MeV)	Proton energy range (MeV)
			Inclination (°)	Altitude (km)			
PET (SAMPEX)	1.7	58	82	520–670	0–90	1–4 4–20	19–28 28–64
IDP (DEMETER)	1.2	32	98	710	90	0.07–2.4	
MEPED (NOAA)	0.1	30	99	805–855	0–90, 90–0	0.03–2.5	0.03–6.9

3. Particle precipitation from the Van Allen Belts

The characteristics of the trapped particles detected by the satellite detector depend strongly on the position of the satellite, in particular different processes may be responsible for the observed particle precipitation. Examples of EM interactions that strongly affect the couplings within the troposphere–ionosphere–magnetosphere system, and are possible processes for particle precipitation, are the solar wind, changes of electric and magnetic field distributions, heat flows and small-scale interactions. EM emissions observed in the circum-terrestrial environment consist of a superposition of natural emissions and several anthropogenic EM noises. Also, some natural events at the Earth's surface such as thunderstorm activity, earthquakes and volcanic eruptions can generate EM signals detected onboard the LEO satellites.

3.1 *Van Allen Belts*

Trapped particles follow gyro- and bounce-motion between hemispheres, as well as longitudinal drift, satisfying the adiabatic invariant associated with each periodic motion (Schulz and Lanzerotti 1974). Longitudinal motion of trapped particles is dominated by the energy-dependent gradient-curvature drift (Hudson *et al.* 2008), in opposite directions for electrons and ions, rather than convection, which dominates the lower energy ring current (Kivelson and Russell 1995). During quiet periods, high-energy trapped electrons are distributed into two belts divided by the electron slot at $L = 2.5$, where L is the drift shell parameter, around which energetic electron flux is relatively low. The SAMPLEX satellite has provided a long-term global picture of the radiation belts (Vassiliadis *et al.* 2002). While the outer radiation belt ($L > 2$) varies with the solar cycle, semiannual and solar rotation time scales as well with geomagnetic storms, the inner belt ($L < 2$) appears to have only solar cycle variations (Russell and Thorne 1970). The inner belt is not in a stationary zone but is affected by the influence of the magnetic activity, and magnetic stroms can induce sudden electron flux enhancements for more than one order of magnitude near $L = 2$.

A key point is to verify that contamination by very energetic ion flux and significant transport of electron flux from the outer belt can be excluded. For this purpose, the NOAA satellite detectors allow an appropriate observation of particle dynamics and fluxes within a large L range and a comparison between the outer and inner radiation belts within the storm duration (Obara *et al.* 2000). Since during great storms it is difficult to distinguish the flux enhancement in the inner belt from the injection of particles from the outer belt, it is particularly interesting to investigate the variability of the electron flux in the inner belt during small and moderate storms (Tadokoro *et al.* 2007). The typical duration of this phenomenon is of 1 day from the start of the main phase up to the early recovery phase of the magnetic storms.

The phenomenology of a magnetic storm on the inner radiation belt can be explained through the pitch-angle scattering near the magnetic equator, which results in a lowering of the belts, and of the particle mirror points, which in turn induces particle precipitation (Larkina *et al.* 1983). It has been suggested that the higher energy component of the electron flux in the inner belt increases more than the lower energy component during magnetic storms. In the SAA, the lower mirror points determine a well-known larger flux enhancement due to a deep particle precipitation into the atmosphere (Sgrigna *et al.* 2005). Consequently, the inclusion or the exclusion of the SAA region in the statistical studies must be carefully evaluated.

3.2 *Loss processes*

Coulomb scattering of the high-energy electrons with thermal particles can account for the observed electron lifetimes close to the earth ($L < 1.25$) (Walt 1996). One of the principal loss processes that control the electron-trapped population in the inner belt is the Whistler-induced electron precipitation (WEP) (Rodger 2003). The magnitude of a typical WEP event that determines the overall importance of WEP to radiation belt losses can be calculated from theoretical analysis (Abel and Thorne 1998b) or evaluated from experimental observations, such as in situ measurements of WEP events (Voss *et al.* 1998).

Whistler-mode waves are naturally generated during lightning discharges in the atmosphere. VLF emissions of lightning is made up of spherics and whistlers. Spherics are coincident with the optical lightning stroke and can be measured at distances of several thousand kilometres from the original lighting stroke, as they are trapped in the ground-ionosphere wave-guide. Whistlers are EM waves with a continuous tone that begin at low frequencies (~10 kHz) and rapidly decrease in frequency ending at VLF (several hundred Hz) within a few seconds. Whistlers propagate into the plasmasphere (Helliwell *et al.* 1973), along ducted and non-ducted paths. Ducted whistlers follow the geomagnetic field lines since they are refracted within a density enhancement of ionospheric plasma along the field line. A larger number of lightning bolts produce non-ducted whistlers that propagate into the plasmasphere and are not constrained to follow the geomagnetic field lines (Inan *et al.* 1989). There have been many observations reporting that individual lightning can cause the precipitation of energetic electrons from the Van Allen Belts (VABs) (Bortnik *et al.* 2006). Lightning-induced electron precipitation (LEP) events are also produced by non-ducted lightning whistlers (Green *et al.* 2005). The phase and amplitude perturbation induced by LEP events in VLF receivers are referred to as Trimpis.

The cyclotron resonant coupling with trapped electrons is mainly efficient near the equatorial zone (Tsurutani and Lakhina 1997). Due to multiple interactions with whistler mode waves, an electron pitch angle will approach 0° (Millan and Thorne 2007). Consequently, resonant electrons are moved into the bounce loss cone and lost by the radiation belts. Due to collisions with particles in the lower ionosphere or upper atmosphere, the electrons will precipitate into the atmosphere (Rycroft 1973). Since globally the flux of particle precipitation can vary over more than a factor of 10, whereas the time-dependent local rate can vary over nearly 3 orders of magnitude, the monitoring of precipitation rates is essential to predict the thermospheric weather. An upper limit on stably trapped electron and proton fluxes was established (Kennel and Petchek 1966) based on pitch angle scattering losses to the atmosphere induced by circularly polarized EM waves.

Modulated precipitation of energetic electrons induced by modulated transmissions from the narrowband phase modulation (24 kHz) transmitter was recently observed and determined to be relatively small (about 2×10^{-4} ergs s^{-1} cm^{-2} at $L \sim 2$) compared with LEP events (Inan *et al.* 2007). Fluxes of energetic electrons can induce whistlers through the Cerenkov process, both during a geomagnetic storm and in conjunction with the seismic activity. Data of whistler-wave propagation collected by ground-based observatories have indicated that whistlers with anomalous dispersion coefficients are probably correlated with earthquakes occurring along the whistler propagation geomagnetic field line. It was supposed to be a possible influence of seismicity on the propagation of magnetospheric whistler waves at low altitudes (Hayakawa *et al.* 1993).

4. NOAA data analysis and results

A NOAA archive record (Evans and Greer 2004) contains 32 seconds of data, including a full set of orbital parameters provided every 8 seconds; in addition, satellite latitude and longitude are provided every 2 seconds. The database comprises 16 full data collection cycles from the MEPED electron and proton telescope instruments, so they are provided every 2 seconds; we point out that these are sampled for 1 second every 2 seconds. A selected portion of the SEM-2 instrument status, temperature and system health data as well as data quality and ancillary information are included. The first step in the preparation of the data consisted of the transformation of all binary files into Ntuples (Couet and Goossen 1998) and simultaneously applying selections and including additional information.

A measure of the general level of daily geomagnetic activity over the globe indicated by the Ap index and abnormally high ionospheric plasma ionizations due to solar flares indicated by sudden ionospheric disturbances (SID) were included in the Ntuples. Data were downloaded respectively from the National Geophysical Data Center (NGDC) at ftp://ftp.ngdc.noaa.gov/STP/GEOMAGNETIC_DATA/APSTAR/apindex and from the American Association of Variable Star Observers (AAVSO) at http://www.aavso.org/observing/programs/solar/sidbase/. Furthermore, we added the minimum mirror point altitudes using the UNILIB libraries (Krunglanski 2002) to determine whether particles were precipitating.

As all sets of orbital parameters are provided every 8 seconds, we chose this value as the basic time step for our study. Consequently all other variables were defined with respect to the 8-second step. Thus, 8-second averages of CRs, latitude, longitude, MEPED and omni-directional data were calculated. Unreliable CRs with negative values were labelled and excluded from the analysis. Since the energy detected for the electrons is a cumulative sum over three thresholds equal to $E_1 = 30$ keV, $E_2 = 100$ keV and $E_3 = 300$ keV, we redefined the energy channels derived from the difference of the energies thresholds to obtain electrons detected in the intervals 30–100, 100–300 and >300 keV, which are similar to the proton energy channels. Unreliable CRs were defined and excluded when $E_2 - E_1 < 0$ and $E_3 - E_2 < 0$.

4.1 *Continuous PB selection*

Our analysis method followed the strategy introduced in 2005 for the analysis of SAMPEX data with some modifications (Fidani and Battiston 2008). These modifications were necessary since NOAA satellites operate at higher orbits and cover different energy range intervals. We calculated the daily averages of CRs and then defined particle bursts (PBs) as the condition for which a CR fluctuation was not due to statistical fluctuations with a probability equal to 99%. We then proceeded to fill the Ntuples with the PB information; with respect to the previous analysis, we also defined contiguous PBs, i.e. series of continuous PBs.

The averages were calculated in each cube of a three-dimensional matrix defined by L-shell, pitch angle α and geomagnetic field B. The L-shell bin was set at 0.1 as in past cases (Sgrigna *et al.* 2005) and the range was set between 0.9 and 2.2, so that we had 13 intervals. In this study, the pitch angle is equal to the difference between the particle telescope axis and the geomagnetic field directions. The SEM-2 detectors have a finite aperture of 30°; we chose a bin of 15° for a total of 12 intervals. The geomagnetic bin was fixed to be B dependent with shorter intervals going through the radiation belts, because we needed to compensate for the non-linear increase of CRs

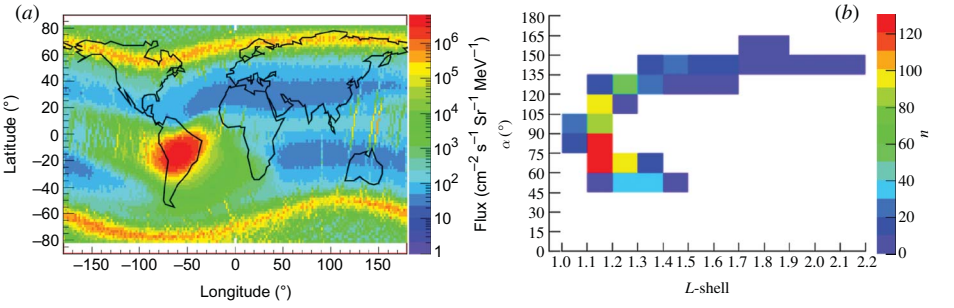

Figure 1. Examples of geographical and invariant surface coordinates. (*a*) The average annual electron flux recorded by the 30–100 keV, 0° MEPED of the NOAA-15 satellite in 2004. (*b*) CR daily average of data cell filling in adiabatic coordinates. n = satellite passes through the same cell.

when the satellite goes through the SAA. The nine B intervals are the following: 16.0–17.5, 17.5–19.0, 19.0–20.5, 20.5–22.0, 22.0–25.0, 25.0–29.0, 29.0–33.0, 33.0–37.0 and 37.0–41.0 μT. The three-dimensional matrix (L,α,B) was then used to calculate averages. To obtain a sufficient statistics we did not consider CRs and CR daily averages relative to cells in which the satellite passed fewer than 20 times. Figure 1(*a*) shows an average annual geographical distribution. We distinguished clearly the SAA region where VABs extend down to the atmosphere and through the satellite altitude; the same behavior recurs at the poles. Figure 1(*b*) shows the average daily CR data filling of the adiabatic intervals for every geomagnetic cell where B = 22–25 μT.

In figure 2(*a*), the black area shows the geographical satellite locations corresponding to observed particle precipitation, while the red area shows the satellite positions corresponding to a cell where B = 22–25 μT, $1.1 < L < 1.2$ and $90° < \alpha < 105°$. Figure 2(*b*) shows a typical 8-second CR distribution corresponding to the same cell.

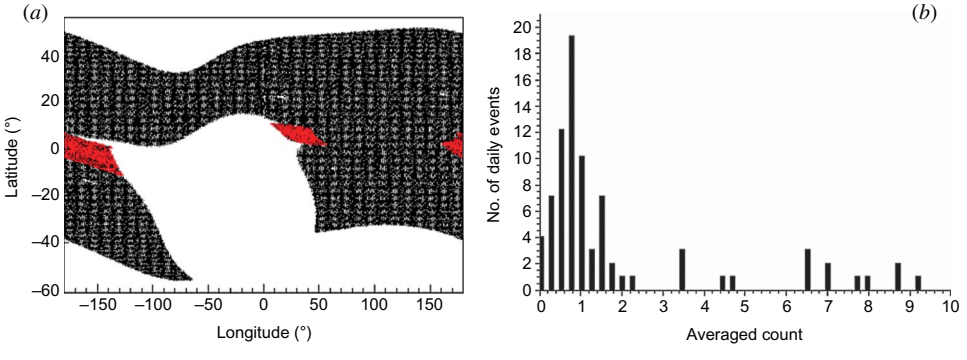

Figure 2. Examples of CR spatial distribution and statistics. The red area in (*a*) is the geographic region corresponding to a cell selected from the figure 1(*b*), which produces the distribution on figure 2(*b*). The black area is the region where the mirror point altitudes are less than 100 km for L-shells below 2.2. In (*b*) the distribution counts averaged in 8 seconds on 26 December 2004, for 0° electrons with energy from 30 to 100 keV, $1.1 < L < 1.2$, $90° < \alpha < 105°$ with 22 μT $< B <$ 25 μT.

The CR distribution is compatible with a Poisson distribution in agreement with earlier works (Sgrigna *et al.* 2005). As done previously (Fidani and Battiston 2008), to define the condition for which a CR is a non-poissonian fluctuation with 99% probability, we introduced the number of variances that the amplitude of the CRs must exceed the average value.

Continuous PBs were defined from 8-second PBs by simply joining a continuous set of PBs, up to a maximum duration of 600 seconds. Because the VABs are densely populated and strongly influenced by solar activity, we were interested in anomalous particle fluxes outside VABs detected during solar quiet days. The NOAA satellites pass through the VABs inside the SAA and polar regions, thus these regions can be excluded by selecting the minimum L-shell bouncing altitude <100 km and L <2.2, respectively, which corresponds to the black area of figure 2(*a*). Figures 3 and 4 are a summary of the electron PB activity during 11 years in the NOAA-15 database. These data refer to the 0° detector, with electron energies from 30 to 100 keV.

4.2 *PBs and solar activity*

Particles that are affected by EM perturbations experience L variation and if they belong to the inner VABs they may fall into the atmosphere. Particle precipitation from the lower boundary of the radiation belts can be described as a result of pitch-angle diffusion and drifting around the Earth along an L-shell (Abel and Thorne 1998a). In this process, the altitude of the bouncing points decreases, and when the particles fall below 100 km they interact with the atmosphere and are lost. With the UNILIB subroutines we calculated the minimum L-shell bouncing altitudes H_{mirror} and recorded them in the Ntuples so that we could select particle precipitation events by the condition H_{mirror} <100 km. In figures 3 and 4, continuously precipitating PBs are shown in black to identify quiet solar periods (Ap < 16 and SID = 0) and in grey for the solar perturbed periods (Ap > 15 and SID = 1). A nearly 11-year solar period shows an inverse correlation with the PB number. An additional correlation between the PBs and the boreal summer is also seen. In fact, even if no solar storms were observed in these periods, a seasonal influence emerges during the period of low solar activity.

We wondered whether a method to eliminate similar solar and other astronomical influences from selected PBs existed in order to show a correlation with Earth-like phenomena such as earthquakes. We would like to eliminate any possible influences from extraterrestrial sources and orbiting dynamics. Apart from the Sun, extraterrestrial sources that could influence particle precipitation (Mandea and Balasis 2006) are astrophysical objects with exceptional activity and strong and coherent energy emissions, capable of travelling enormous distances. Such objects are astrophysical sources monitored by a large number of detectors from the Earth and also from space. We can thus discard their effects on the NOAA database, as we already discussed in Fidani and Battiston (2008).

4.3 *PBs autocorrelation*

A time series containing non-random patterns can be studied using a correlation function. An autocorrelation PB analysis is used in order to study the effects of solar modulation versus orbital parameters on the PB activity. Figure 5 shows a complete account of 11 years of PB autocorrelation for 0° electrons, for both the 8 second and contiguous cases. This was done by considering only solar quiet days from figures 3 and 4. When we calculate the correlation with earthquakes, it is important to take

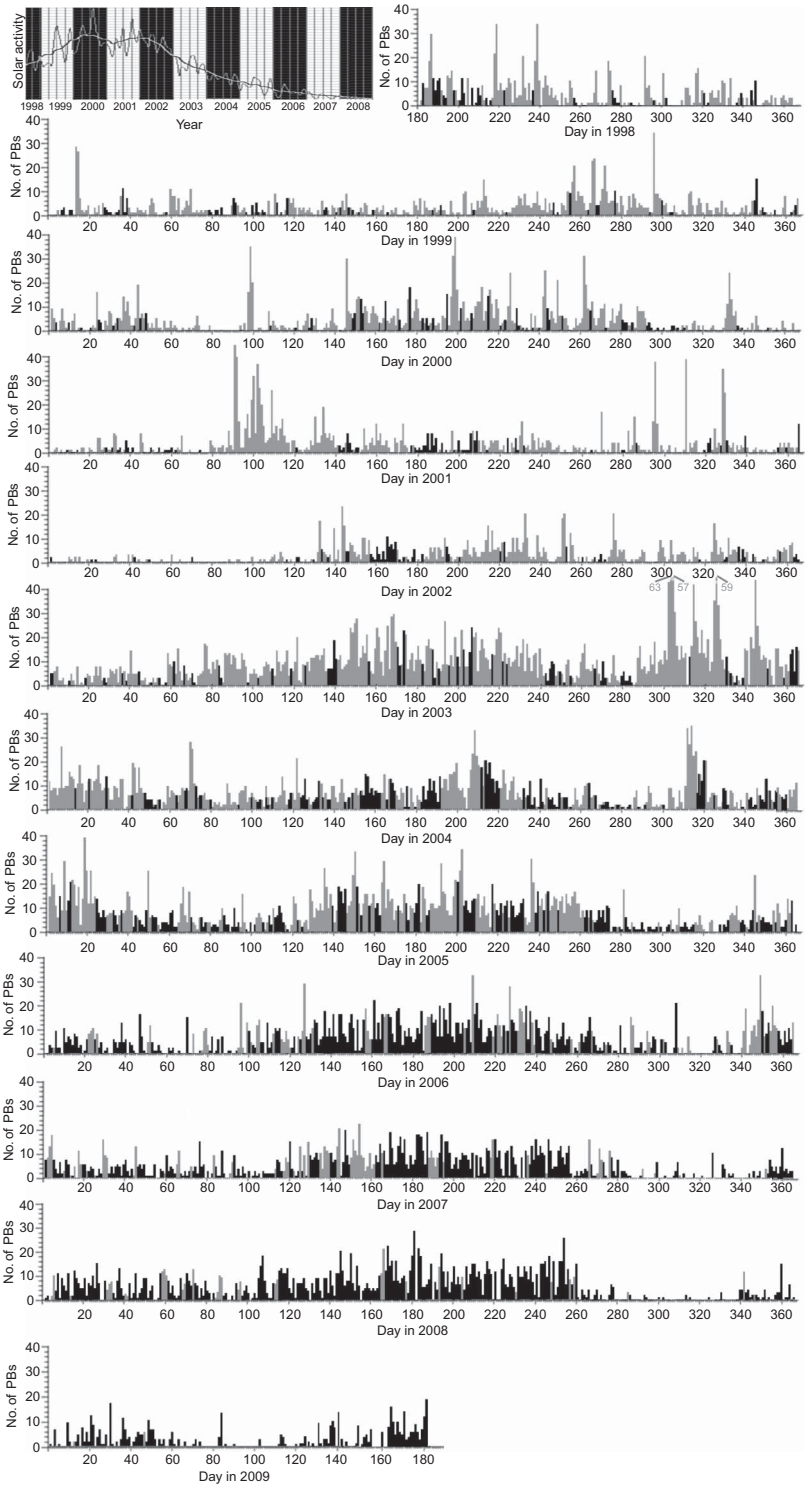

Figure 3. Time series from 1998 to the first 6 months of 2009 of contiguous burst activity from the NOAA-15 database. Grey colour indicates days with Ap > 15 or SID = 1.

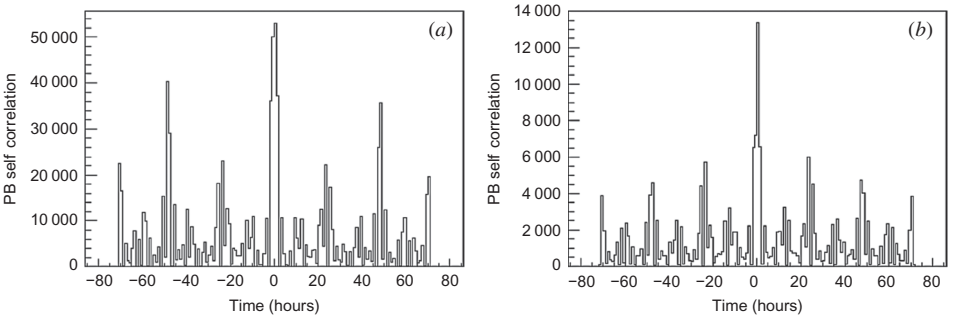

Figure 4. PB autocorrelation distribution of the NOAA-15 PB database with Ap < 16 and SID = 0; (*a*) 8 seconds bursts; (*b*) continuous bursts.

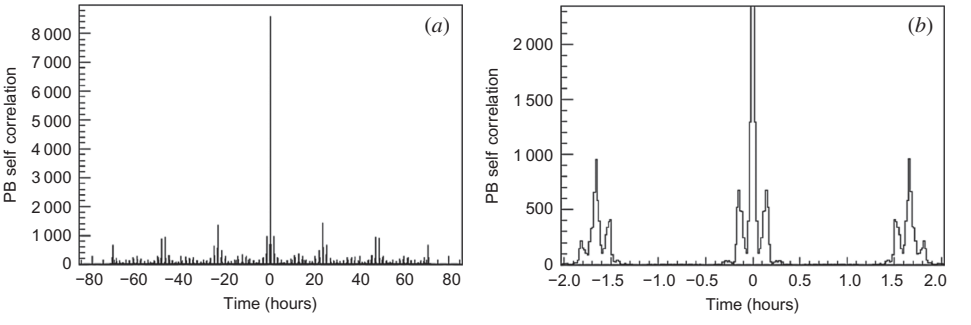

Figure 5. Continuous PB autocorrelation distribution of NOAA-15 PB database with AP < 16 and SID = 0; (*a*) 72 hours autocorrelation interval; (*b*) 2 hours autocorrelation interval.

into account the autocorrelation since its structure is sensitive to contributions from orbital periods.

To better analyse the physical origin of such behaviour, we plot the contiguous PB autocorrelation with finer bins (n/min), shown in figure 6. The plots in figure 6 reveal additional periods that contribute to PB autocorrelations. In summary, we observe three periods: around 8–9 minutes, 100 minutes and 24 hours. The 100-minute period is the orbital period of the NOAA satellite. This period highlights that additional PBs are often recorded after one satellite revolution. This is due to the existence of an extended active region over the equator, westward of the SAA, where particle detectors systematically meet high fluxes. The 24-hour period indicates that the satellite crosses the same geographical region because it is on a heliosynchronous orbit that rotates once a day; a 12-hour period stands out because the opposite position of each orbit is still crossing the equator. The difference between the amplitudes at 24- and 12-hour periods could be a sunny dark side effect. The peaks around 8–9 minutes depend on the geometry of the 'active' region near the equator, namely, the splitting of the green stripe west of the SAA in figure 1(*a*). This is due to the shape of VAB crossing the satellite altitude close to the SAA. Detector temporal recordings show a two-peak function as shown in a previous work (Fidani and Battiston 2008). The temporal distance between the two peaks is equal to the satellite time interval necessary to cross VAB bouncing regions, which is around 8–9 minutes at low latitudes.

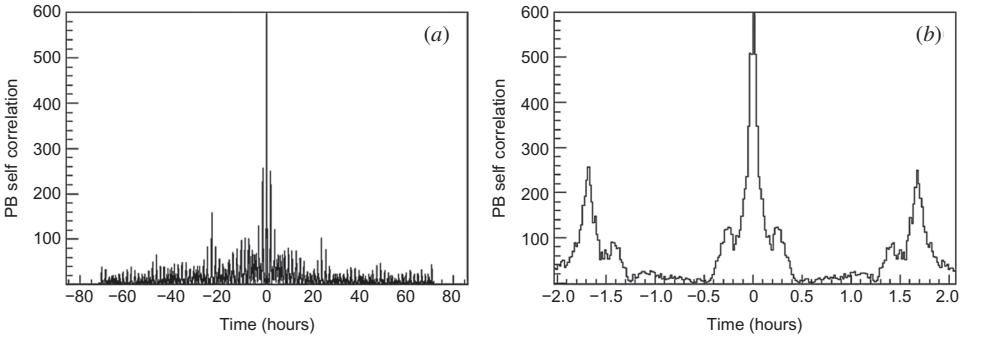

Figure 6. Continuous PB autocorrelation distribution of NOAA-15 PB database with Ap > 50 and SID = 1; (*a*) 72 hours autocorrelation interval; (*b*) 2 hours autocorrelation interval.

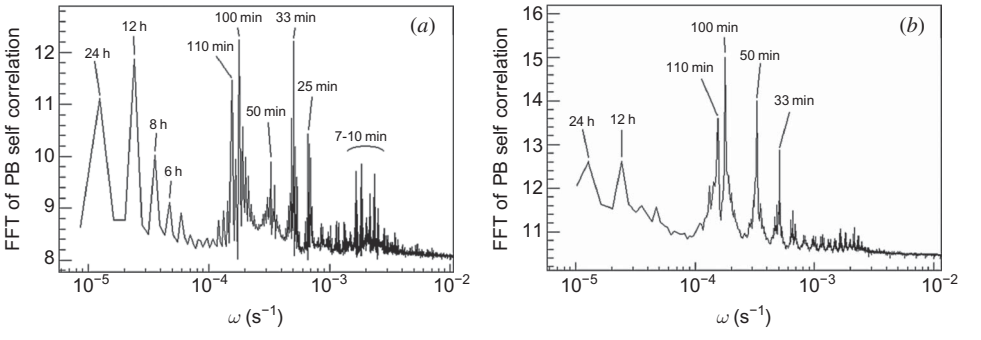

Figure 7. FFT of autocorrelation functions; (*a*) for Ap < 15; (*b*) for Ap > 30.

The plots in figure 7 show the autocorrelation function when solar activity was high, Ap > 50 and SID = 1. We observe several differences between these plots and those in figure 5. First, it is asymmetric and has higher peaks on the negative time. This means that the rising time of the particle precipitation phenomenon is less than the decreasing one. Second, the spectrum changes significantly. From figure 7(*a*), we can still clearly see the 24-hour and the 100-minute periods, while the 12-hour period slowed down to 10 hours; from figure 7(*b*) we see that the periods around 8–9 minutes disappeared. High geomagnetic periods are characterized by strong precipitation of particles, especially near the SAA. In this situation, the lower VABs became full of particles and the satellite detected PBs in all of the bands between the two bouncing points near the equator. So double peaks corresponding to the bouncing points become less important and ultimately disappear. For the same reason, the precipitation area increases during the same periods and in the opposite orbital positions giving rise to periods shorter than 12 hours.

4.4 *Spectral composition analysis*

Since we would like to discard the solar influence on PB precipitation and to study Earth links to VABs, we wonder if it is possible to use spectral analysis to do so. We performed a fast Fourier transform (FFT) of the autocorrelation function for Ap ≤ 15 and plotted it on figure 8(*a*). Several harmonics appeared; we could recognize 24 hours

plus four principal harmonics, about 100 minutes plus three principal harmonics. Shorter times are better resolved; from figure 8 we can observe that they consist of six times: 6, 7, 8, 9, 10 and 11 minutes, and they disappear as solar activity increases. This process is due to the detection of PBs without a double peak near the equator as previously explained. If we study the solar influence on these peaks, we discover that the Sun begins to influence PB activity when Ap > 15, confirming the validity of our previous analysis (Fidani and Battiston 2008). We conclude that FFT analysis of PB autocorrelation is useful for determining when solar influence starts; we can use it to quantify solar influence on inner VAB as well.

Figure 8(*a*) shows the peaks of the PB autocorrelation spectrum, which comes from orbital satellite parameters and VAB geometry crossing satellite positions. The PB autocorrelation spectrum helps us to better spot periods that could be found in the correlation function with other phenomena. Some peaks are of a few hours; they indicate periods completely similar to that discovered in earthquake–PB correlation (Aleksandrin *et al.* 2003, Sgrigna *et al.* 2005). Thus, we would consider the necessary steps for disentangling PB autocorrelation from the orbital forcing, in order to eliminate the possibility of misleading correlations. For this we could treat the autocorrelation as due to the convolution of two contributions, one being the PB evolution $f(t)$ and the other the orbital forcing $g(t)$ in time t. The convolution theorem states that the Fourier transform of a convolution of two functions $f(t) * g(t)$ is equal to the product between the Fourier transforms of the functions $F(\omega)G(\omega)$, where ω is the frequency. One way we can calculate the PB evolution is by an inverse FFT of

$$F(\omega) = \frac{\mathcal{F}(f(t) * g(t))}{G(\omega)}, \tag{1}$$

where $F(\omega)$ is the Fourier transform of $f(t)$ and $G(\omega)$ can be derived from the autocorrelation spectra by considering the orbital forcing. For example, we could assume that particle detection occurs within a few minutes during the satellite orbit on a precise latitude and longitude interval. We could assume that such a detection has a Gaussian efficiency along these orbit segments. Furthermore, we could assume that the $G(\omega)$ spectra are defined by the main frequencies detected from the autocorrelation FFT:

$$G(\omega) = \sum_n A_n \exp\left[-B_n(\omega - \omega_n)^2\right], \tag{2}$$

where ω_n are the main frequencies, A_n are the relative intensities and B_n are the Gaussian widths. Under these assumptions a reconstruction of the PB time structure, which is corrected from orbital modulations and is obtained by inverse FFT, is possible.

4.5 *Multiple observations*

Particle detection is only one of the space observations from satellites. Several measurements are already included in the same satellite, for example, DEMETER (Parrot 2002) or NOAA (Davies 2007), and planned in future payloads. A better satellite study efficiency should be obtained with a precise ordering and interlink among measurements. For this we suggest thinking about three kinds of measurements from satellite instruments with respect to earthquake-prone areas. These can be classified as follows.

- Measurements at the locations of the satellite position, which give us the physical state of the ionosphere: temperature, composition and concentration of plasma, quasi-static electric and magnetic fields and wide band EM waves.
- Measurements that connect the Earth's surface to the satellite give us the physical states of lithosphere and the bottom layer of the atmosphere under or between satellite positions: GPS phases, infrared emissions and optical images of clouds.
- Measurements that come from space to the satellite position give us the physical states of the magnetosphere and heliosphere: particle precipitation from the VAB and cosmic rays.

Each payload usually covers several different measurements; however, being that the scope is to study a unique process, we expect to find that measurements are linked.

Plasma analysers should be capable of detecting weak disturbances, such as those induced by EM waves recorded in the ionosphere, which comprise low drift, together with EM fields at the satellite position to completely define the physical situation (Berthelier *et al.* 2006). GPS can be used to evaluate the total electron content (TEC; Liu *et al.* 2004) along the path between the satellite and surface positions or among different satellites (Trigunait *et al.* 2004). This is useful for probing the space between satellites and the Earth's surface and for finding a causal link between the first and second kind of measurements. On the other hand, the collection of infrared emissions, optical images and other meteorological quantities in a large angular view (Singh *et al.* 2007) constitutes the first step towards determining the influence of seismic phenomena on the ionosphere. Particle detectors are reliable instruments for space, thanks to recent missions (Casolino and PAMELA 2008); they should be able to detect the type, energy, pitch angle and rates of high energy particles (Battiston *et al.* 2007). Instrumental sensibility should be adequate for those fluxes that are capable of producing expected ionization, which explains TEC and plasma variations (Rothkaehl *et al.* 2006), again making it possible to determine a causal link among different measurements. In this framework, the non-linear dynamics should be evaluated for possible ion-acoustic soliton connections (Mofiz and Battiston 2009).

The first kind of space measurement is a local one, although it can reflect the tectonic, meteorological and anthropogenic situation under the satellite position. Satellites need several days to pass the same position along their orbits; being so, every measurement will be a finite sampling of the physical variables concerning a definite region of the ionosphere. In this case, a better sampling system will require a larger number of satellites to be employed and working separately.

The second kind of measurements take complete advantage of the satellite's far-field point of view and thus are capable of sampling the same surface portion of the Earth over 1 day. Furthermore, linked observations to Earth-like radio and GPS stations, as well as to other satellites, will be considered to sample the paths between their positions. In this case, a finite number of satellites will be either used separately or used in alternately working pairs.

The third kind of measurement must take into account the strictly connected phenomena of particle motion and geomagnetic field dynamics, so that it is possible to define adiabatic invariants, which are the better variables for ordering particle measurements (Walt 1994). In this ordering, satellite acquisition systems would realize a whole sampling of the adiabatic variable space in a few hours. Moreover, polar orbit satellites are favourites because they cover the whole adiabatic invariant space, giving a picture of all the VABs. Here, a small number of satellites will be required to obtain a satisfactory scanning of the magnetosphere.

5. Conclusions

We analysed the temporal series of the NOAA particle database defining continuous PB activity and we reported about one complete solar cycle influence on particle precipitation from VABs. Earthquake and earth-like influence on PBs can be discovered only if data are free from the Sun's influence. For this we selected a finite portion of satellite space and time measurements from the global database. Bounded measurements in space and time, which are periodic, being shaped by orbital parameters, introduce a periodical modulation in PB activity, which must be taken into account when looking for earth-like phenomena. A method was proposed that consists of studying the autocorrelation function of PBs with FFT. We discovered several harmonics in PB autocorrelation which are linked to orbital periods of NOAA satellites, their orientation with respect to the Sun and the crossing of the orbital geometry with the VAB shape. Solar influence on PBs was defined by considering the disappearance of a group of harmonics in the PB autocorrelation function.

The study of the FFT autocorrelation function revealed several harmonics smaller than 24 hours. We underline the importance to understand such harmonics in order to avoid misleading conclusions on statistical correlations of particle precipitation with other phenomena. Finally, we stress the importance of this approach in the study of other satellite measurements which are subject to similar reduced space-time collections due to orbital conditions.

5.1 *Satellite constellation*

A LEO point of view permits the continuous observation of very large areas of the planet, but it cannot be globally guaranteed using only a single satellite. For this reason, satellite constellations have been considered for future missions in order to thoroughly monitor ionospheric and magnetospheric earthquake associations. Satellite payloads suited for these constellations have already been designed by the Italian (ESPERIA) (Sgrigna *et al.* 2007), Russian (VULKAN) (Pulinets 2006) and Chinese (CSES) (Xuhui *et al.* 2007) projects. These satellites also include a detailed measurement of bursts of energetic particles.

To improve these kinds of studies, we would need to define the satellite constellation parameters to determine optimal on-board data processing, data transmission and data sharing. For that, after we have decided all the useful measurements and their limiting parameters, we should define:

- the number of satellites, their orbit parameters and include the types of detectors to cover the whole planetary surface, stressing that not all detectors will be necessarily on-board every satellite;
- a common protocol for data exchange to provide the opportunity to constitute a shared database that needs to be homogeneous and suitable for multivariate analysis; the first measurement kind will need a low data rate transmission, the second kind will need a moderate data rate transmission; the third kind will need a higher data rate;
- additional variables that are not measured but are calculated from existing and tested models such as the International Geomagnetic Field reference (IGRF) and UNILIB, which are needed for the geomagnetic field, atmosphere density and composition; Geometry and Tracking (GEANT4) and the Space Environment Information System (SPENVIS) for particle space simulations; similarly, the

database can include solar spectral emissions, solar wind data such as velocity and composition, which can be extracted from the Geostationary Operational Environmental Satellite (GOES) or other solar mission databases; 3-hour Ap, Kp (a weighted average of disturbances in the horizontal component of earth's magnetic field) and Disturbance Storm Time (DST) indexes must be taken into account because of solar influence on the geomagnetic field while SID and modern cosmic ray satellites need to be considered for cosmic rays influence.

These configurations have already been utilized in various missions but they have never been considered in the context of a multimission project to date.

5.2 *Final requirements*

Earthquakes are global dangers and the efforts of a single nation hardly meet the requirement to develop a satellite constellation. Given this, it is important to develop common tools and strategies to search for and study these effects; at the same time, create an international scientific community that would support and develop these strategies. The increased amount of data will in turn increase the need for a shared global database to increase the efficiency of the analysis. It will be of the essence to organize a series of meetings of expert scientists in the fields of satellite instrumentation and both ionospheric and earthquake phenomena in order to establish the best configuration for the data collected. This will include measurement and storage protocols to allow for the creation of an international database that will lead to an improved exploitation of future missions devoted to these studies.

References

Abel, B. and Thorne, R.M., 1998a, Electron scattering loss in earths inner magnetosphere 1. Dominant physical processes. *Journal of Geophysical Research*, **103**, pp. 2385–2396.

Abel, B. and Thorne, R.M., 1998b, Electron scattering loss in earths inner magnetosphere 2. Sensitivity to model parameters. *Journal of Geophysical Research*, **103**, pp. 2397–2407.

Aguilar, M. and AMS-2 Collaboration, 2002, The Alpha Magnetic Spectrometer (AMS) on the International Space Station I: results from the test flight on the Space Shuttle. *Physics Reports*, **366**, pp. 331–405; 2003, Erratum, **380**, pp. 97–98.

Aleksandrin, S.Yu., Galper, A.M., Grishantzeva, L.A., Koldashov, S.V., Maslennikov, L.V., Murashov, A.M., Picozza, P., Sgrigna, V. and Voronov, S.A., 2003, High-energy charged particle bursts in the near-Earth space as earthquake precursors. *Annales Geophysicae*, **21**, pp. 597–602.

Bakaldin, A.V., Batishchev, A.G., Voronov, S.A., Galper, A.M., Grishantseva, L.A., Koldashov, S.V., Naumov, P.Yu., Chesnokov, V.Yu. and Shilov, V.A., 2007, Satellite experiment ARINA for studying seismic effects in the high-energy particle fluxes in the earths magnetosphere. *Cosmic Research*, **45**, pp. 445–448.

Baker, D.N., Mason, G.M., Figueroa, O., Colon, G., Watzin, J.G. and Aleman, R.M., 1993, An overview of the Solar, Anomalous, and Magnetospheric Particle Explorer (SAMPEX) Mission. *IEEE Transaction on Geoscience and Remote Sensing*, **31**, pp. 531–541.

Battiston, R., Conti, L., Picozza, P. and Sgrigna, V., 2007, Earthquake monitoring from space 10 years of R&D in Italy. In *Proceedings of the International Workshop*, 25–27 July 2007, Jakarta, Indonesia, pp. 36–48.

Berthelier, J.J., Godefroy, M., Leblanc, F., Seran, E., Peschard, D., Gilbert, P. and Artru, J., 2006, IAP, the thermal plasma analyzer on DEMETER. *Planetary and Space Science*, **54**, pp. 487–501.

Bhattacharya, S., Sarkar, S., Gwal, A.K. and Parrot, M., 2009, Electric and magnetic field perturbations recorded by DEMETER satellite before seismic events of the 17th July 2006 M 7.7 earthquake in Indonesia. *Journal of Asian Earth Sciences*, **34**, pp. 634–644.

Bortnik, J., Inan, U.S. and Bell, T.F., 2006, Temporal signatures of radiation belt electron precipitation induced by lightning-generated MR whistler waves: 2. Global signatures. *Journal of Geophysical Research*, **111**, A02205, doi:10.1029/2005JA011398.

Casolino, M. and PAMELA Collaboration, 2008, Magnetospheric and solar physics observations with the PAMELA experiment. *Nuclear Instruments and Methods in Physics Research A*, **588**, pp. 243–246.

Casolino, M., Picozza, P. and On BEHALF of the PAMELA collaboration, 2008, Launch and commissioning of the PAMELA experiment on board the Resurs-DK1 satellite. *Advances in Space Research*, **41**, pp. 2064–2070.

Cook, V.R., Cummings, A.C., Cummings, J.R., Garrard, T.L., Kecman, B., Mewaldt, R.A., Selesnick, R.S., Stone, E.C., Baker, D.N., von Rosenvige, T.T., Blake, J.B. and Callis, L.B., 1993, PET: a proton/electron telescope for studies of magnetospheric, solar and galactic particles. *IEEE Transaction on Geoscience and Remote Sensing*, **31**, pp. 565–571.

Couet, O. and Goossens, M., 1998, *HBOOK Statistical Analysis and Histogramming Reference Manual* (Geneva: Information Technology Division, CERN).

Davies, K. and Baker, D.M., 1965, Ionospheric effects observed around the time of the Alaskan earthquake of March 28. *Journal of Geophysical Research*, **70**, pp. 2251–2253.

Davis, G., 2007, History of the NOAA satellite program. *Journal Applied Remote Sensing*, **1**, 012504, doi:10.1117/1.2642347.

Dobrovolsky, I.P., Zubkov, S.I. and Miachkin, V.I., 1979, Estimation of the size of earthquake preparation zones. *Pure and Applied Geophysics*, **117**, pp. 1025–1044.

Evans, D.S. and Greer, M.S., 2004, Polar Orbiting Environmental Satellite Space Environment Monitor - 2: instrument descriptions and archive data documentation. *NOAA Technical Memorandum January*, version 1.4 (Silver Spring, MD: NOAA).

Fidani, C. and Battiston, R., 2008, NOAA particle analysis with seismic activity. *Natural Hazard Earth System Science*, **8**, pp. 1277–1291.

Freund, F., 2000, Time-resolved study of charge generation and propagation in igneus rocks. *Journal of Geophysical Research*, **105**, pp. 11001–11019.

Green, J.L., Boardsen, S.A., Garcia, L., Taylor, W.W., Fung, S.F. and Reinisch, B.W., 2005, On the origin of whistler mode radiation in the plasmasphere. *Journal of Geophysical Research*, **110**, A03201, doi:10.1029/2004JA010495.

Hayakawa, M., Yoshino, T. and Morgounov, V.A., 1993, On the possible influence of seismic activity on the propagation of magnetospheric whistlers at low latitudes. *Physics of Earth Planetary Interior*, **77**, pp. 97–108.

Helliwell, R.A., Katsufrakis, J.P. and Trimpi, M.L., 1973, Whistler induced amplitude perturbation in VLF propagation. *Journal of Geophysical Research*, **78**, pp. 4679–4688.

Hudson, M.K., Kress, B.T., Mueller, H.-R., Zastrow, J.A. and Blake, J.B., 2008, Relationship of the Van Allen radiation belts to solar wind drivers. *Journal of Atmospheric and Solar-Terrestrial Physics*, **70**, pp. 708–729.

Inan, U.S., Golkowski, M., Casey, M.K., Moore, R.C., Peter, W., Kulkarni, P., Kossey, P., Kennedy, E., Meth, S. and Smit, P., 2007, Subionospheric VLF observations of transmitter-induced precipitation of inner radiation belt electrons. *Geophysical Research Letters*, **34**, L02106, doi:10.1029/2006GL028494.

Inan, U.S., Walt, M., Voss, H.D. and Imhof, W.L., 1989, Energy spectra and pitch angle distributions of lightning-induced electron precipitation: analysis of an event observed on the S81–1 (SEEP) satellite. *Journal of Geophysical Research*, **94**, pp. 1379–1401.

Kennel, C.F. and Petchek, H., 1966, Limit on stably trapped particle fluxes. *Journal of Geophysical Research*, **71**, pp. 1–28.

Kivelson, M.G. and Russell, C.T., 1995, *Introduction to Space Physics*. (New York: Cambridge University Press).

Krunglanski, M., 2002, UNILIB Reference Manual. *Belgisch Instituut Voor Ruimte – Aeronomie*. Available online at: http://www.oma.be/NEEDLE/unilib.php/

Larkina, V.I., Migulin, V.V., Nalivaiko, A.V., Gershenzon, N.I., Gokhberg, M.B., Liperovsky, V.A. and Shalimov, S.L., 1983, Observations of VLF emission, related with seismic activity on the Interkosmos-19 satellite. *Geomagnetism and Aeronomy*, **23**, pp. 684–687.

Liu, J.Y., Chuo, Y.J., Shan, S.J., Tsai, Y.B., Pulinets, S.A. and Yu, S.B., 2004, Pre-earthquake ionospheric anomalies registered by continuous GPS TEC measurements. *Annales Geophysicae*, **22**, pp. 1585–1593.

Mandea, M. and Balasis, G., 2006, The SGR 1806-20 magnetar signature on the Earths magnetic field. *Geophysical Journal International*, **167**, pp. 586–591.

Millan, R.M. and Thorne, R.M., 2007, Review of radiation belt relativistic electron losses. *Journal of Geophysical Research*, **69**, pp. 362–377.

Mofiz, U.A. and Battiston, R., 2009, Possible ion-acoustic soliton formation in the ionospheric perturbations before Puer earthquake observed on DEMETER. *Earthquake Science*, **22**, pp. 257–262.

Nemec, F., Santolik, O. and Parrot, M., 2009, Decrease of intensity of ELF/VLF waves observed in the upper ionosphere close to earthquakes: a statistical study. *Journal of Geophysical Research*, **114**, A04303, doi:10.1029/2008JA013972.

Obara, T., Den, M., Miyoshi, Y. and Morioka, A., 2000, Energetic electron variation in the outer radiation zone during early May 1998 magnetic storm. *Journal of Atmospheric Solar-Terrestrial Physics*, **62**, pp. 1405–1412.

Parrot, M., 1995, Use of satellites to detect seismo-electromagnetic effects. *Advances in Space Research*, **15**, pp. 27–35.

Parrot, M., 2002, The micro satellite DEMETER. *Journal of Geodynamics*, **33**, pp. 535–541.

Pulinets, S.A., 2006, Space technologies for short-term earthquake warning. *Advances in Space Research*, **37**, pp. 643–652.

Rodger, C.J., 2003, Subionospheric VLF perturbations associated with lightning discharges, *Journal of Atmosferic Solar-Terrestrial Physics*, **65**, pp. 591–606.

Rothkaehl, H., Bucik, R. and Kudela, K., 2006, Ionospheric plasma response to the seismic activity. *Physics and Chemistry of the Earth*, **31**, pp. 473–481.

Russell, T. and Thorne, M., 1970, On the structure of the inner magnetosphere Christopher. *Cosmic Electrodynamics*, **1**, pp. 67–89.

Rycroft, M.J., 1973, Enhanced energetic electron intensities at 100 km altitude and a whistler propagating through the plasmasphere. *Planetary and Space Science*, **21**, pp. 239–251.

Sarkar, S., Gwal, A.K. and Parrot, M., 2007, The radiation belts. *Journal of Atmospheric and Solar-Terrestrial Physics*, **69**, pp. 1524–1540.

Sauvaud, J.A., Moreau, T., Maggiolo, R., Treilhou, J.-P., Jacquey, C., Cros, A., Coutelier, J., Rouzaud, J., Penou, E. and Gangloff, M., 2006, High-energy electron detection onboard DEMETER: the IDP spectrometer, description and first results on the inner belt. *Planetary and Space Science*, **54**, pp. 502–511.

Schulz, M. and Lanzerotti, L.J., 1974, *Particle Diffusion in the Radiation Belts* (New York: Springer).

Sgrigna, V., Buzzi, A., Conti, L., Picozza, P., Stagni, C. and Zilpimiani, D., 2007, Seismo-induced effects in the near-earth space: combined ground and space investigations as a contribution to earthquake prediction. *Tectonophysics*, **431**, pp. 153–171.

Sgrigna, V., Carota, L., Conti, L., Corsi, M., Galper, A.M., Koldashov, S.V., Murashov, A.M., Picozza, P., Scrimaglio, R. and Stagni, L., 2005, Correlations between earthquakes and anomalous particle bursts from SAMPEX/PET satellite observations. *Journal of Atmospheric and Solar-Terrestrial Physics*, **67**, pp. 1448–1462.

Singh, R.P., Cervone, G., Singh, V.P. and Kafatos, M., 2007, Generic precursors to coastal earthquakes: inferences from Denali fault earthquake. *Tectonophysics*, **431**, pp. 231–240.

Tadokoro, H., Tsuchiya, F., Miyoshi, Y., Misawa, H., Morioka, A. and Evans, D.S., 2007, Electron flux enhancement in the inner radiation belt during moderate magnetic storms. *Annales Geophysicae*, **25**, pp. 1359–1364.

Trigunait, A., Parrot, M., Pulinets, S. and Li, F., 2004, Variations of the ionospheric electron density during the Bhuj seismic event. *Annales Geophysicae*, **22**, pp. 4123–4131.

Tsurutani, B.T. and Lakhina, G.S., 1997, Some basic concepts of waveparticle interactions in collisionless plasmas. *Review of Geophysics*, **35**, pp. 491–501.

Varotsos, P., 2001, A review and analysis of electromagnetic precursors phenomena. *Acta Geophysica Polonica*, **107**, pp. 1–42.

Vassiliadis, D., Klimas, A.J., Kanekal, S.G., Baker, D.N. and Weigel, R.S., 2002, Long-term-average, solar cycle, and seasonal response of magnetospheric energetic electrons to the solar wind speed. *Journal of Geophysical Research*, **107**, pp. 1383–1401.

Voss, H.D., Walt, M., Imhof, W.L., Mobilia, J. and Inan, U.S., 1998, Satellite observations of lightning-induced electron precipitation, *Journal of Geophysical Research*, **103**, pp. 725–744.

Walt, M., 1994, *Introduction to Geomagnetically Trapped Radiation*, p. 168 (Cambridge: Cambridge University).

Walt, M., 1996, Source and loss processes for radiation belt particles. In *Radiation Belts: Models and Standards*. *Geophysical Monograph*, J.F. Lemaire, D. Heynderickx and D.N. Backer (Eds.), Vol. 97, pp. 1–13 (Washington, DC: American Geophysical Union).

Xuhui, S., Shaoxie, X., Yun, W., Xinjian, S., Dongmei, Y., Jingfa, Z., Khunli, K., Xuebin, D., Jianhai, D., Jiadong, Q., Feng, J. and Lanwei, W., 2007, General proposal for China Seismo-Electromagnetic Satellite project, early warming and monitoring earthquake by using electromagnetism detecting satellite. In *Proceedings of the International Workshop*, 25–27 July 2007, Jakarta, Indonesia, p. 14.

Yurur, M.T., 2006, The posititive temperature anomaly as detected by Landsat TM data in the eastern Marmara Sea (Turkey): possible link with the 1999 Izmit earthquake. *International Journal of Remote Sensing*, **27**, pp. 1205–1218.